analytical chemistry

pubs.acs.org/ac

Technical Note

# Electrotransfer of Immunoprobes through Thin-Layer Polyacrylamide Gels

Andoni P. Mourdoukoutas and Amy E. Herr*

Cite This: *Anal. Chem.* 2022, 94, 2706−2712

Read Online

ACCESS | Metrics & More | Article Recommendations | Supporting Information

Downloaded via UNIV OF CALIFORNIA BERKELEY on October 13, 2022 at 19:13:21 (UTC).
See https://pubs.acs.org/sharingguidelines for options on how to legitimately share published articles.

**ABSTRACT:** Hydrogels are important structural and operative components of microfluidic systems, finding diverse utility in biological sample preparation and interrogation. One inherent challenge for integrating hydrogels into microfluidic tools is thermodynamic molecular partitioning, which reduces the in-gel concentration of molecular solutes (e.g., biomolecular regents), as compared to the solute concentration in an applied solution. Consequently, biomolecular reagent access to in-gel scaffolded biological samples (e.g., encapsulated cells, microbial cultures, target analytes) is adversely impacted in hydrogels. Further, biomolecular reagents are typically introduced to the hydrogel via diffusion. This passive process requires long incubation periods compared to active biomolecular delivery techniques. Electrotransfer is an active technique used in Western blots and other gel-based immunoassays that overcomes limitations of size exclusion (increasing the total probe mass delivered into gel) and expedites probe delivery, even in millimeter-thick slab gels. While compatible with conventional slab gels, electrotransfer has not been adapted to thin gels (50−250 $\mu$m thick), which are of great interest as components of open microfluidic devices (vs enclosed microchannel-based devices). Mechanically delicate, thin gels are often mounted on rigid support substrates (glass, plastic) that are electrically insulating. Consequently, to adapt electrotransfer to thin-gel devices, we replace rigid insulating support substrates with novel, mechanically robust, yet electrically conductive nanoporous membranes. We describe grafting nanoporous membranes to thin-polyacrylamide-gel layers via silanization, characterize the electrical conductivity of silane-treated nanoporous membranes, and report the dependence of in-gel immunoprobe concentration on transfer duration for passive diffusion and active electrotransfer. Alternative microdevice component layers—including the mechanically robust, electrically conductive nanoporous membranes reported here—provide new functionality for integration into an increasing array of open microfluidic systems.

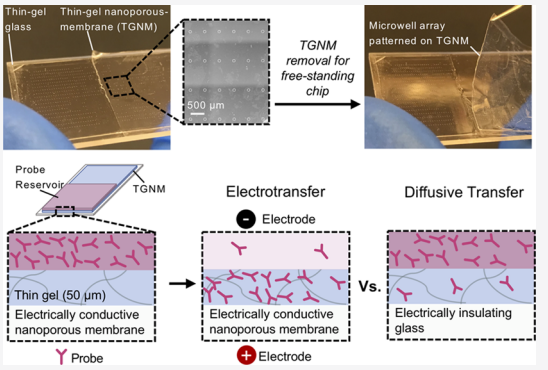


The integration of hydrogels into microfluidic systems facilitates broad device functionality, finding utility in cell encapsulation and microbial culturing platforms,[1,2] drug and gene delivery vehicles,[3−5] and diagnostic tools.[6−10] Hydrogels are gaining prominence as microdevice component layers, because hydrogels are biologically inert,[11,12] can be molecularly functionalized with a variety of molecule types (e.g., biomolecules such as extracellular matrix proteins and nonbiological photoactivatable cross-linkers),[13,14] and can be fabricated into 3D physical structures with high fidelity.[1,15] An emerging class of hydrogel-based microfluidic devices utilizes delicate thin-gel layers (50−250 $\mu$m thick) grafted onto centimeter-scale, mechanically robust support substrates (glass, plastic). Such "open" microfluidic devices (vs enclosed microchannel-based devices) reduce barriers to reagent exchange, as biomolecule solutions can be directly interfaced with functional regions of the gel layer without migrating through microchannel networks.[2,6,9,16,17]

However, the total biomolecule mass that can be delivered to a hydrogel suffers from inefficient diffusive-driven biomolecule delivery to gel, as small gel pores impede loading of large macromolecules into the gel matrix.[18−20] Specifically, the loading of biomolecules into a hydrogel matrix by passive diffusion alone is hindered by size-exclusion partitioning, which reduces the diffusive equilibrium concentration of biomolecules in a hydrogel matrix compared to their concentration in free solution.[18] Inefficient biomolecule loading to hydrogels adversely impacts (i) total drug mass loaded to delivery vehicles,[16] (ii) cellular transfection in culturing platforms,[5] and (iii) immunoprobe mass available for target−probe immunocomplex formation in diagnostic assays.[18,21]

To increase the total biomolecule mass loaded to millimeter-scale hydrogel devices, electrotransfer has been developed to

**Received:** September 9, 2021
**Accepted:** January 25, 2022
**Published:** February 3, 2022


© 2022 American Chemical Society

https://doi.org/10.1021/acs.analchem.1c03919
*Anal. Chem.* 2022, 94, 2706−2712

actively transfer immunoprobes into slab gels[22] as well as cleared tissue samples[23] and transfer proteins from digested tissue slices into layered hydrogel stacks in layered electrophoretic transfer.[24] Drawing inspiration from gel-to-membrane (PVDF, nitrocellulose) protein electrotransfer used in conventional and microfluidic Western blotting,[25−27] electrotransfer drives biomolecule delivery to a gel by applying an electric field across an electrically conductive, freestanding stack of a biomolecule (e.g., immunoprobe) reservoir layered onto a hydrogel device. Conducting an electrical current through the entirety of the immunoprobe reservoir and hydrogel device stack is required for electrotransfer. Electrotransfer has thus primarily seen application to freestanding and slab gels, including millimeter-thick gels that are mechanically robust and maintain structural integrity without being grafting to a rigid support substrate.[22,23,28] As a result, electrotransfer is yet to be extended to delicate thin-gel layers that require grafting onto mechanically robust, yet electrically insulating support substrates. To expand the applicability of electrotransfer to emerging thin-gel-based microfluidic systems, there is a need to offer a more functional substrate alternative to replace electrically insulating glass, including performance that is mechanically robust, electrically conductive, and still well-suited for imaging analyses.

Here, we introduce a fabrication method for a microdevice component layer composed of a thin-gel layer grafted to a nanoporous membrane that supports rapid and increased delivery of biomolecules to the thin-gel layer by electrotransfer. In developing this "thin-gel nanoporous-membrane" (TGNM) chip, we reengineer the conventional thin-gel chip to support electrotransfer probe loading by grafting the thin gel to an electrically conductive nanoporous-membrane support substrate (instead of an electrically insulating glass slide) via novel nanoporous-membrane silanization and chip fabrication methods. Using antibody probes as a model biomolecule species, we additionally establish engineering design rules for mitigating diffusive probe losses during electrotransfer probe loading and characterize the electrical conductivity of silane-treated nanoporous membranes. Finally, we demonstrate that our electrically conductive TGNM chip supports rapid electrotransfer probe loading and results in greater probe mass loading to the thin-gel layer in less time compared to loading of probe by diffusion alone.

## EXPERIMENTAL SECTION

**Nanoporous-Membrane and Glass Slide Silanization.** To facilitate covalent binding of polyacrylamide gel (10%T, 3.5C) to the nanoporous membranes (regenerated cellulose, Spectra Por RC Dialysis Tubing, 3.5 kDa MWCO, #132725T), a nanoporous-membrane silanization method was developed with inspiration from glass slide silanization protocols[29] and fabrication techniques for hybrid gel−cellulose materials.[30−32] A detailed procedure of nanoporous-membrane and glass slide silanization is described in the Supporting Information.

**Fabrication Process for the TGNM Chip.** A detailed procedure of experimental operation is provided in the Supporting Information. A brief overview of the fabrication steps is included here and in Figure 1: (i) layering a hydrated nanoporous membrane onto a glass slide and allowing the nanoporous membrane to adhere to the glass slide by drying, (ii) applying a polyacrylamide gel precursor solution onto an SU-8 micropost patterned silicon wafer, (iii) placing the nanoporous-membrane glass slide assembly onto the gel precursor solution and allowing the gel to polymerize, covalently binding to the nanoporous membrane, (iv) removing the polymerized TGNM glass slide assembly from the wafer and peeling away the TGNM chip from the glass support.

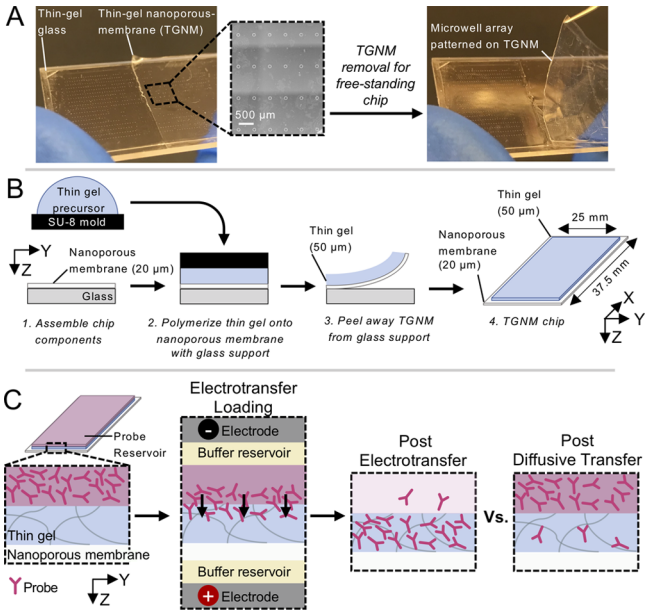


**Figure 1.** Design of a thin-gel nanoporous-membrane (TGNM) chip that is mechanically robust and electrically conductive for electrotransfer delivery of a probe to thin-gel layers. (A) Bright-field image of a TGNM chip first supported by a glass slide and then removed from the glass slide to produce a freestanding TGNM chip. (B) Thin polyacrylamide gel layers are grafted onto nanoporous membranes using silanization chemistry atop an SU-8 mold that patterns microwells into the thin-gel layer. To polymerize the thin-gel layers onto nanoporous membranes, a polyacrylamide gel precursor was cast in a layered assembly involving a full glass slide, a nanoporous membrane, a polyacrylamide precursor solution, and an SU-8 mold. (C) Immunoprobe is loaded into the TGNM chip by electrotransfer, to offer improved mass loading of the probe more quickly.

**Electrical Conductivity Measurements.** The electrical conductivity measurements were performed using an "out-of-plane" electrotransfer configuration composed of two 1× Tris-glycine buffer reservoirs. A detailed procedure of experimental operation is provided in the Supporting Information.

**Probe Loading Experiments and Image Analysis.** The electrotransfer and diffusive-driven probe loading experimental, imaging, and analysis procedures are described in the Supporting Information.

## RESULTS AND DISCUSSION

Electrotransfer probe loading in the TGNM chip is facilitated by grafting a thin gel (50−250 $\mu$m thick) onto a nanoporous membrane (Figure 1A,B). Conventionally, thin gels are grafted onto support substrates (e.g., glass, GelBond) to prevent thin-gel layer deformation during assay performance. Here, the nanoporous membrane prevents thin-gel layer deformation but is electrically conductive. The mechanically robust, electrically conductive TGNM chip supports delivery of probe molecules into the thin-gel layer by electrotransfer for (i) increased total probe mass in thin gel and (ii) rapid probe delivery, compared to diffusion alone (Figure 1C).


https://doi.org/10.1021/acs.analchem.1c03919
Anal. Chem. 2022, 94, 2706−2712

**Minimizing Probe Loss by Diffusion during Probe Loading.** We first sought to understand diffusive probe losses from open thin-gel layers during electrotransfer probe loading. As probe molecules electromigrate through the thin gel, the molecules undergo three-dimensional diffusion. Diffusive losses of probe molecules from the thin gel can occur as probe molecules diffuse out of the thin gel into the surrounding environment. We thus aimed to design an electrotransfer configuration to minimize the diffusive loss of probe during electrotransfer loading of probe to the thin gel. We evaluated diffusive probe losses in two electrotransfer configuration designs: an "out-of-plane" electrotransfer configuration (Figure 2A) and an "in-plane" electrotransfer configuration (Figure 2B). As the support substrate in the "out-of-plane" configuration is in the electrical current path, there is a design need for the support substrate to be electrically conductive. In contrast, the electrical current path in the "in-plane" configuration does not traverse through the support substrate, and the configuration is thus compatible with existing electrically nonconductive support substrates.

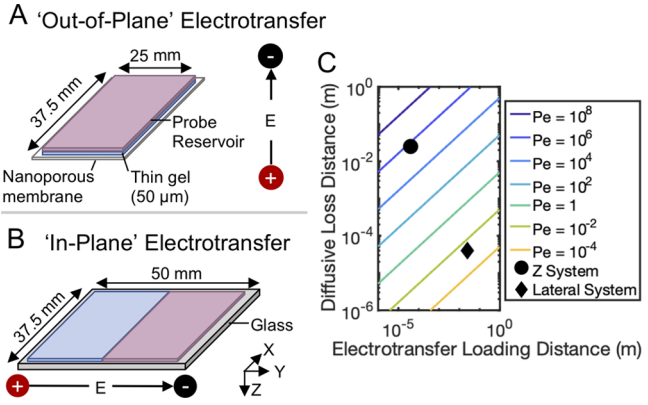


**Figure 2.** Peclet analysis of electrotransfer configurations indicates an "out-of-plane" design minimizes diffusive probe loss during electrotransfer loading. (A) Schematic showing the "out-of-plane" electrotransfer configuration. (B) Schematic showing the "in-plane" electrotransfer configuration. (C) A Peclet analysis of electrotransfer probe loading shows that the Peclet number in the "out-of-plane" configuration is ~$10^8$× greater than in the "in-plane" configuration.

To assess the diffusive loss of probe expected during electromigration in the "out-of-plane" and "in-plane" electrotransfer configurations, we defined a Peclet number ($Pe$) as the ratio of the time for diffusive probe loss from the thin gel ($t_D$) to the time to electrotransfer probe into the thin gel ($t_E$). The $Pe$ number for the "in-plane" configuration ($P_{Lateral}$) is given by

$$Pe_{Lateral} = \frac{t_D}{t_E} = \frac{\left[\frac{Z^2}{2 \cdot D}\right]}{\left[\frac{Y}{\mu \cdot E}\right]}$$

where $Z$ is the thin-gel thickness (50 $\mu$m), $D$ is the diffusion coefficient of probe in the thin gel (1.40 $\mu m^2$/s, Note S1), $Y$ is the width of the thin gel (25 × $10^3$ $\mu$m), $\mu$ is the electrophoretic mobility of probe in the thin gel (1.81 × $10^3$ $\mu m^2$/(V s), previously determined[22]), and $E$ is the applied electric field (100 V/cm). The $Pe$ for the "out-of-plane" configuration ($Pe_Z$) is calculated as

$$Pe_Z = \frac{t_D}{t_E} = \frac{\left[\frac{Y^2}{2 \cdot D}\right]}{\left[\frac{Z}{\mu \cdot E}\right]}$$

We anticipated that due to the disproportional length scales of the thin-gel layer thickness in $Z$ (50 $\mu$m) compared to the mm-scale length and width of the thin-gel layer in $X$ and $Y$ (25 × $10^3$ $\mu$m and 37.5 × $10^3$ $\mu$m), electrotransfer loading of probe in the "out-of-plane" configuration would minimize expected diffusive losses.

Results of this analysis are presented in Figure 2C and indicate that the Peclet number in the "out-of-plane" electrotransfer configuration is ~$10^8$× greater than in the "in-plane" configuration. The disproportionate transport distances (in $Z$ vs $X$–$Y$) minimize diffusive probe losses in the "out-of-plane" electrotransfer configuration, as (i) the electromigration distance, and thus probe loading time, is shortest in the $Z$-axis, and (ii) the migration distances for diffusive losses are longest in the $X$- and $Y$-axes. The $Pe$ analysis in electrotransfer probing thus provides a design rule for minimizing diffusive probe losses and indicates that minimal losses occur in the "out-of-plane" electrotransfer configuration.

**Investigating the Fidelity of the TGNM Chip Fabrication Process.** As the nanoporous membranes had not been previously demonstrated as a thin-gel support substrate, we aimed to assess the fidelity of the TGNM chip fabrication process in comparison to conventional thin-gel glass chip fabrication. To aid in fidelity assessments, we pattern microwell features into the thin-gel layer of both chip types and compare dimensions of the microwell feature across chips. We anticipated that there would be no significant difference in the dimensions of microwell features patterned into the TGNM and thin-gel glass chips.

The TGNM and thin-gel glass chips were fabricated with a fluorescent dye (rhodamine B) included in the gel precursor solution to visualize polymerized gel features and allow for comparison between the two chip types (Figure 3A,B; additional information provided in the Supporting Information). To mitigate the introduction of new sources of nonspecific binding between antibodies and the nanoporous membrane (in comparison nonspecific binding events occurring between antibody and glass in existing thin-gel–glass chips), we silanize the nanoporous membranes using the same silane molecule, 3-(3-(trimethoxysilyl)propyl methacrylate), used to silanize glass in thin-gel glass chips.[29] Furthermore, to prevent antibody migration through the membrane or physical entrapment within the membrane, we select a membrane with a 3.5 kDa molecular weight cutoff, well-below the 150 kDa molecular mass of IgG antibodies. Fluorescence in the gel was imaged by confocal microscopy. We anticipated that rhodamine B would be present in both the thin-gel and nanoporous-membrane layers, as the molecular mass of rhodamine B (~472 Da) is below the molecular mass cutoff of the nanoporous membrane (3.5 kDa). To perform a statistical analysis of the fidelity of the TGNM fabrication process, we quantify the height and diameter of eight microwell structures across the TGNM chip (Supporting Information).

We observe no significant difference in the height and diameter of the microwell structure between thin gels fabricated in thin-gel glass chips and TGNM chips ($n$ = 8, $p$ > 0.05 for both dimensions, Mann–Whitney U-test, Figure


https://doi.org/10.1021/acs.analchem.1c03919
Anal. Chem. 2022, 94, 2706–2712

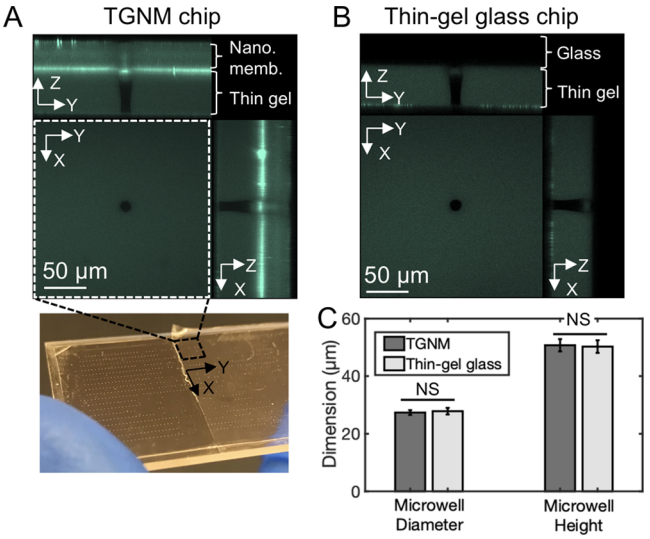


**Figure 3.** Microwell patterning into TGNM chips. Fluorescent confocal microscopy images of a single microwell in a thin-gel layer composed of (A) TGNM and (B) thin-gel glass. Rhodamine B fluorescence shown in turquoise. (C) The TGNM fabrication technique does not perturb the height and diameter of individual microwells compared to the conventional thin-gel glass chip fabrication technique ($n$ = 8, $p$ > 0.05 for both dimensions, Mann−Whitney U-test).

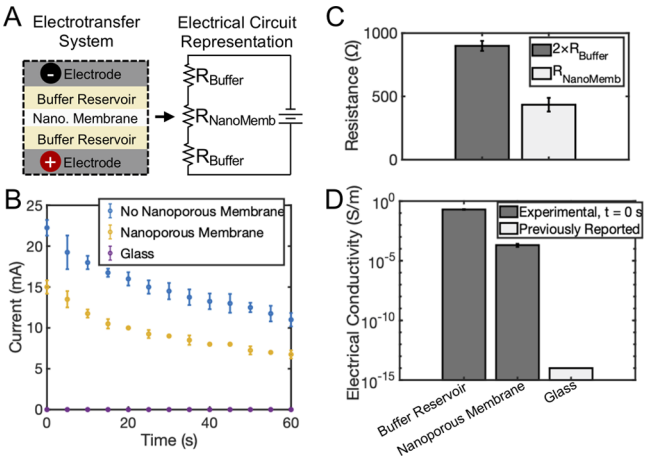


**Figure 4.** Electrical properties of the nanoporous membrane (after silanization) in comparison to the buffer reservoir (buffer-soaked filter paper) and glass. (A) Schematic of the electrotransfer configuration (not to scale) and an electrical circuit analogue. (B) Electrical current over time through the electrotransfer configurations composed of two buffer reservoirs sandwiching either (i) no nanoporous membrane, (ii) nanoporous membrane (after silanization), or (iii) glass. (C) Resistance of each layer of the electrotransfer configuration is determined using the electrical circuit analogue. (D) The electrical conductance of the buffer reservoir and nanoporous membrane are calculated and compared to previously reported glass electrical conductivity values ($n$ = 4 per condition, $p$ < 0.05, Mann−Whitney U-test).

3C). Interestingly, rhodamine B molecules appear to aggregate at the interface of the thin-gel and nanoporous-membrane layers in the TGNM chip. We attribute the rhodamine B aggregation at the interface between the thin-gel and nanoporous-membrane layers to nonspecific hydrophobic interactions between rhodamine B and the silane present on the nanoporous-membrane surface.[33]

**Assessment of Nanoporous-Membrane Electrical Conductivity after Silanization.** We next sought to characterize the electrical conductivity of the nanoporous membranes after silane treatment. To do so, we used an "out-of-plane" electrotransfer configuration composed of three layers: two identical buffer reservoirs that sandwich a material under investigation (nanoporous membrane, glass, or no nanoporous membrane). A constant voltage was applied to the electrotransfer configuration, and the configuration can be represented by an electrical circuit, in which each material layer is described by a resistor in series (electrotransfer conditions described in Supporting Information; Figure 4A).

As expected, no electrical current was detected in the electrotransfer configuration that included a glass layer (Figure 4B). This supports our understanding of the incompatibility of thin-gel glass chips with electrotransfer probing. We observe that the initial electrical current ($t$ = 0 s) for the nanoporous-membrane configuration is 67.2 ± 5.1% of the initial electrical current of the configuration with no nanoporous membrane ($n$ = 4, $p$ < 0.05, Mann−Whitney U-test; Figure 4B). The final electrical current ($t$ = 60 s) in the nanoporous-membrane configuration is 67.2 ± 8.9% of the final electrical current of the no nanoporous-membrane configuration ($n$ = 4, $p$ < 0.05, Mann−Whitney U-test; Figure 4B). We additionally observe that the electrical current decays over the 60 s of applied constant voltage in both of the electrotransfer configurations that included either the nanoporous membrane or no nanoporous membrane (Figure 4B). The decay in electrical current is attributed to products of electrolysis and Joule heating (SI Note 3),[22,34,35] and further study would build on the engineering design of similar electrotransfer systems to mitigate the impact of Joule heating and electrolysis on electrical current stability.[22,28,24]

To next establish the intrinsic electrical conductivity of the nanoporous membrane, we calculated the electrical conductivity of the nanoporous membrane using the initial electrical current ($t$ = 0 s). Using the electrical circuit representation in Figure 4A, we first calculated the resistance at $t$ = 0 s of the individual buffer reservoir, $R_{Buffer}$, and the nanoporous membrane, $R_{NanoMemb}$, and find that $R_{Buffer} \approx R_{NanoMemb}$ (Figure 4C). Thus, for the electrotransfer configuration including a nanoporous membrane (Figure 4A), the total resistance of the two buffer reservoirs is twice as large as the total resistance of the single nanoporous membrane, as shown in Figure 4C. To calculate the electrical conductivity of the nanoporous membrane and the buffer reservoir layers, we scale $R_{Buffer}$ and $R_{NanoMemb}$ by the dimensions of each material layer and observe ~$10^3$× lower electrical conductivity of the nanoporous membrane than the buffer reservoir (material dimensions described in Supporting Information; Figure 4D). Importantly, while the nanoporous membrane is less electrically conductive than the buffer reservoir, the nanoporous membrane is quite thin (20 $\mu$m vs 2 × $10^3$ $\mu$m per buffer reservoir), and thus, the total resistance of the nanoporous-membrane layer is comparable to the resistance of each buffer reservoir at $t$ = 0 s. We additionally note that our experimentally determined electrical conductivity of the nanoporous membrane is >$10^{10}$× greater than the previously reported electrical conductivity of glass.[36] Ultimately, we demonstrate the silanized nanoporous membrane to be an electrically conductive support substrate alternative to glass (and other electrically insulating materials) for thin-gel devices.


https://doi.org/10.1021/acs.analchem.1c03919
Anal. Chem. 2022, 94, 2706−2712

**Electrotransfer Probe Loading to TGNM Chips.** After understanding the electrical conductivity characteristics of the TGNM, we investigated the TGNM compatibility with electrotransfer probe loading to gel using donkey anti-rabbit Alexa-Fluor 647 as a model probe species and a TGNM that was not previously exposed to any protein. We hypothesized that electrotransfer probe loading (as compared to probe loading by diffusion) would result in (i) an expedited time scale of probe delivery to the thin-gel layer and (ii) an increased total mass of probe delivered to the thin-gel layer. To evaluate the performance of electrotransfer probe loading, TGNM chips were fabricated as described in Figure 1, and the electrotransfer configuration shown in Figure 5A was

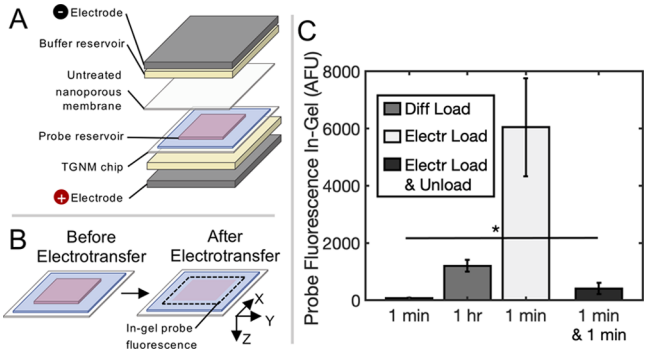


**Figure 5.** Electrotransfer probe loading to the TGNM chip results in an increased total probe mass in the thin-gel layer and reduced time scales of probe delivery. (A) Schematic of the assembly used in electrotransfer probe loading to the TGNM chip. (B) Fluorescent probe delivered into the thin-gel layer is measured by imaging the surface of the TGNM chip after electrotransfer. (C) Electrotransfer probe loading for 1 min results in a greater amount of probe delivered to the thin-gel layer than diffusive probe loading for 1 min and 1 h. Probe that is loaded to the thin-gel layer by 1 min of electrotransfer can be unloaded from the thin-gel layer by 1 min of electrotransfer with reversed electrode polarity ($n = 4$ for each condition, $p < 0.05$ for all pairwise condition comparisons, Mann−Whitney U-test). The probe reservoir contained donkey anti-rabbit Alexa-Fluor-647-labeled IgG antibodies. TGNM chips were not exposed to other proteins.

assembled. To specifically interrogate transport kinetics in probe loading, the TGNM had no previous exposure to protein before probe loading. After loading, the probe was immobilized in gel using a single exposure of UV light and a UV-mediated photocapture chemistry (previously characterized[14]). The probe reservoir is composed of agarose gel (100 $\mu$m thick) and was fabricated by a protocol described in previous electrotransfer probing configurations.[22] Agarose gel was used, as agarose probe reservoirs have been previously demonstrated for rapid fabrication with minimal handling and efficient probe release (minimal probe entrapment in gel) by electrotransfer.[22] Alternative probe reservoir formats may be designed in future studies for improved ease of probe retrieval (e.g., isolated probe solution chambers). To ensure probe electromigration out of the probe reservoir, the following electrotransfer parameters were chosen: 50 V/cm electric field, applied for 1 min. These electrotransfer conditions correspond to probe electromigration in agarose of >300 $\mu$m, >3× greater than the 100 $\mu$m probe reservoir (assumes probe electrophoretic mobility in agarose is $1.16 \times 10^{13}$ $\mu m^2/(V\ s)$, previously characterized[22]). In the diffusive-driven conditions, we replicate conventional diffusive probing strategies in thin-gel glass chips by not removing the TGNM chip from the glass slide support substrate used during chip fabrication (Figure 1B).[29] We anticipate that the thin-gel layers have similar electrical conductivities to the buffer solution, as the hydrogel is >90% fluid by volume (polymer volume fraction < 0.1).[37]

We observe that 1 min of electrotransfer loading results in a 79.9 ± 26.4× greater in-gel probe fluorescence than 1 min of diffusive-driven loading and a 5.01 ± 1.67× greater in-gel probe fluorescence than 1 h of diffusion-driven loading ($n = 4$; $p < 0.05$ Mann−Whitney U-test; Figure 5C). As expected, we see a 15.9 ± 3.9× increase in in-gel probe fluorescence from the 1 min diffusive condition to the 1 h diffusive condition, indicating that 1 min of diffusive-driven transfer is insufficient time to reach the transport equilibrium ($n = 4$, $p < 0.05$ Mann−Whitney U-test; Figure 5C). A Mann−Whitney U-test and sample sizes of $n = 4$ were selected following literature precedent on studies of enhanced probe mass loading to thin-gel−glass chips by gel dehydration[20] and electrotransfer probing in slab gel systems[22] as well as a convention of $n \geq 3$ for computing the standard deviation of empirical results. We next sought to characterize probe entrapment in the TGNM after electrotransfer loading and unloading. To do so, the probe was first loaded via electrotransfer into the TGNM as described above. The probe was then unloaded via electrotransfer from the TGNM by refreshing the buffer reservoirs and reversing the electrode polarity. We observe that after electrotransfer unloading, the probe fluorescence in the TGNM is 6.8 ± 3.7% of the probe fluorescence in TGNM resulting from 1 min of electrotransfer loading. We note this is similar to the performance in slab gel electrotransfer probing systems (~5% probe entrapment in gel after electrotransfer loading and unloading). Collectively, our results support our hypothesis and the engineering design of the TGNM as a system that supports electrotransfer probe delivery to the thin-gel layer, resulting in (i) increased total probe mass in the thin gel and (ii) reduced time scales of probe delivery (compared to conventional diffusive-driven probing). The electrotransfer principle in TGNM was demonstrated as a proof of concept here using 2Ab Dk anti-Rb AF647. We anticipate that this would be applicable to other proteins, particularly antibodies of similar charge and size of the same IgG class (SI Note 2).

We additionally observe an increase in the interchip coefficient of variation (CV) of probe loaded in the TGNM by electrotransfer compared to diffusive-driven loading (28.4% in 1 min electrotransfer, 17.5% in 1 h diffusive). The increase in the CV of the electrotransfer method is in line with previous investigations of enhanced probe mass loading to thin-gel−glass chips by gel dehydration (CV of 24.7%).[20] However, previous electrotransfer probing systems applied to mm-scale hydrogels have achieved <5% CV in total probe loading by mitigating adverse impacts of electrolysis on run-to-run variability[22,28] and may be used to inform future studies of electrotransfer probe loading using TGNM. In particular, (i) pH changes in the buffer reservoir may be prevented by increasing buffering capacity, (ii) temperature variability may be reduced by incorporating robust heat dissipation mechanisms, and (iii) resistivity variability in the buffer reservoir may be mitigated by incorporating a gas bubble removal mechanism.[22,28]

## CONCLUSIONS

We introduced a TGNM chip designed for electrotransfer probe delivery to the thin-gel layer, overcoming a fundamental


https://doi.org/10.1021/acs.analchem.1c03919
Anal. Chem. 2022, 94, 2706−2712

challenge to diffusion-based probe delivery in thin-gel immunoassays. Our design involves performing an analytical investigation of electrotransfer probe loading configurations and establishing a Peclet number as a design guideline for minimizing diffusive probe losses during electrotransfer probe loading. We additionally describe a fabrication method for the novel TGNM chips, involving silane-treating nanoporous membranes for thin polyacrylamide gel layer grafting. Further, we assess key traits of the TGNM chip, including thin-gel layer fabrication fidelity and the electrical conductivity of silane-treated nanoporous membranes. Lastly, we observe 1 min of electrotransfer probe loading in our TGNM chip to result in a ∼80× greater probe delivery than 1 min of diffusive-driven delivery and a ∼5× greater probe delivery than 1 h of diffusive-driven delivery. Future work involves integration of the TGNM and electrotransfer probe loading capability into microfluidic systems, particularly as a microdevice component layer of immunoassay chips. However, several open questions remain before incorporating the TGNM into an immunoassay, including understanding the impact of enhanced probe mass loading (including multiple probe exchange rounds for primary and secondary antibodies) and expedited probe transport time scales (compared to diffusive loading) on immunocomplex formation. While alternative methods for enhanced probe mass loading in thin-gel−glass immunoassay chips have resulted in improved analytical sensitivity of target protein detection,[20] application of the TGNM to target protein detection is required to understand the analytical sensitivity performance (e.g., signal-to-noise ratio of target protein detection) in this system. Additional challenges to TGNM integration in an immunoassay chip include understanding the impact of nonuniform probe delivery on immunoprobing efficiency in a binding assay. Previous investigations on the impact of nonuniform probe delivery to thin-gel−glass chips have found intrachip probe delivery CV (without corrective measures) to be as high as 50%, introducing spatial variability in both immunoprobing efficiency and background.[38] Enhanced probe mass loading to gel (e.g., by electrotransfer or other active methods) can cause probe concentrations to be in excess of target protein concentrations and limit spatial variability in immunoprobing efficiency, though only for certain binding kinetic regimes (antibody concentration ≫ antibody−target protein dissociation constant, $K_D$).[38,21]

## ■ ASSOCIATED CONTENT

### Supporting Information

The Supporting Information is available free of charge at https://pubs.acs.org/doi/10.1021/acs.analchem.1c03919.

Additional experimental details and methods, diffusion coefficient calculations for antibody probes, discussion of electrokinetic theory and electrical current stability in electrotransfer systems (PDF)

## ■ AUTHOR INFORMATION


### Corresponding Author

**Amy E. Herr** − *Department of Bioengineering, University of California, Berkeley, California 94720, United States;* orcid.org/0000-0002-6906-2985; Email: aeh@berkeley.edu

### Author

**Andoni P. Mourdoukoutas** − *The UC Berkeley/UCSF Graduate Program in Bioengineering, University of California, Berkeley, California 94720, United States;* orcid.org/0000-0001-7340-1401

Complete contact information is available at: https://pubs.acs.org/10.1021/acs.analchem.1c03919


### Author Contributions

All authors designed experiments and wrote and have given approval to the final version. A.P.M. performed experiments.

### Notes

The authors declare no competing financial interest.

The Figure [1]C schematic representation of a ∼4× greater probe concentration loaded to the thin-gel layer by electrotransfer compared to diffusive transfer is informed by the experiments reported in Figure [5]C, in which 1 min of electrotransfer loading results in 5.01 ± 1.67× greater gel fluorescence than 1 h of diffusive loading.

## ■ ACKNOWLEDGMENTS

This work was supported by the National Cancer Institute of the National Institutes of Health, Cancer Moonshot award (R33CA225296, to A.E.H.). A.P.M. was supported by a National Institutes of Health training grant (T32GM008155) and a National Science Foundation Graduate Research Fellowship (1106400). Photolithography was performed in the QB3 Biomolecular Nanotechnology Center. The authors are grateful for discussions with all members of the Herr Lab.

## ■ REFERENCES


(1) Berry, S. B.; Zhang, T.; Day, J. H.; et al. *Lab Chip.* **2017**, *17* (24), 4253−4264.
(2) Barkal, L. J.; Theberge, A. B.; Guo, C.-J.; et al. *Nat. Commun. 2016 71.* **2016**, *7* (1), 1−11.
(3) Lin, C. C.; Metters, A. T. *Adv. Drug Deliv Rev.* **2006**, *58* (12−13), 1379−1408.
(4) Lin, C. C.; Metters, A. T. *Pharm. Res.* **2006**, *23* (3), 614−622.
(5) Quick, D. J.; Anseth, K. S. *J. Controlled Release* **2004**, *96* (2), 341.
(6) Wood, D. K.; Weingeist, D. M.; Bhatia, S. N. *Proceedings of the National Academy of Sciences* **2010**, *107* (22), 10008.
(7) Appleyard, D. C.; Chapin, S. C.; Doyle, P. S. *Anal. Chem.* **2011**, *83* (1), 193.
(8) Chung, K.; Wallace, J.; Kim, S.-Y.; et al. *Nature.* **2013**, *497* (7449), 332−337.
(9) Hughes, A. J.; Spelke, D. P.; Xu, Z.; Kang, C.-C.; Schaffer, D. V.; Herr, A. E. *Nat. Methods.* **2014**, *11* (7), 749.
(10) Tanase, C. P.; Albulescu, R.; Neagu, M. *https://doi.org/101586/erm1130* **2011**, *11* (5), 461−464.
(11) Zhang, X.; Li, L.; Luo, C. *Lab Chip.* **2016**, *16* (10), 1757.
(12) Zubtsov, D. A.; Savvateeva, E. N.; Rubina, A. Y.; et al. *Anal. Biochem.* **2007**, *368* (2), 205−213.
(13) Chen, F.; Tillberg, P. W.; Boyden, E. S. *Science (80-).* **2015**, *347* (6221), 543−548.
(14) Dormán, G.; Nakamura, H.; Pulsipher, A.; Prestwich, G. D. *Chem. Rev.* **2016**, *116* (24), 15284−15398.
(15) Pan, Q.; Yamauchi, K. A.; Herr, A. E. *Anal. Chem.* **2018**, *90* (22), 13419.
(16) Slaughter, B. V.; Khurshid, S. S.; Fisher, O. Z.; Khademhosseini, A.; Peppas, N. A. *Adv. Mater.* **2009**, *21* (32−33), 3307−3329.
(17) Kaigala, G. V.; Lovchik, R. D.; Delamarche, E. *Angew. Chemie Int. Ed.* **2012**, *51* (45), 11224−11240.
(18) Park, H.; Johnson, C. S.; Gabriel, D. A. *Macromolecules.* **1990**, *23*, 1548−1553.

(19) Su, A.; Smith, B. E.; Herr, A. E. *Anal. Chem.* **2020**, *92* (92), 875−883.
(20) Vlassakis, J.; Herr, A. E. *Anal. Chem.* **2015**, *87* (21), 11030−11038.
(21) Goodrich, J. A.; Kugel, J. F. *Binding and Kinetics for Molecular Biologists*; Cold Spring Harbor Laboratories Press, 2007.
(22) Mourdoukoutas, A. P.; Grist, S. M.; Herr, A. E. *Anal Methods.* **2020**, *12* (38), 4638.
(23) Kim, S.-Y.; Cho, J. H.; Murray, E.; et al. *Proc. Natl. Acad. Sci. U. S. A.* **2015**, *112* (46), E6274−E6283.
(24) Zhu, L.; Tangrea, M. A.; Mukherjee, S.; Emmert-Buck, M. R. *Proteomics.* **2011**, *11* (5), 883−889.
(25) Towbin, H.; Staehelin, T.; Gordon, J. *Proc. Natl. Acad. Sci.* **1979**, *76* (9), 4350−4354.
(26) Jin, S.; Furtaw, M. D.; Chen, H.; et al. *Anal. Chem.* **2016**, *88* (13), 6703−6710.
(27) Arvin, N. E.; Dawod, M.; Lamb, D. T.; Anderson, J. P.; Furtaw, M. D.; Kennedy, R. T. *Anal methods.* **2020**, *12* (12), 1606.
(28) Grist, S. M.; Mourdoukoutas, A. P.; Herr, A. E. *Nat. Commun. 2020 111.* **2020**, *11* (1), 1−17.
(29) Kang, C-CC; Yamauchi, K. A.; Vlassakis, J.; Sinkala, E.; Duncombe, T. A.; Herr, A. E. *Nat. Protoc.* **2016**, *11* (8), 1508−1530.
(30) Abdelmouleh, M.; Boufi, S.; ben Salah, A.; Naceur Belgacem, M.; Gandini, A. *Langmuir.* **2002**, *18*, 3203−3208.
(31) Abdelmouleh, M.; Boufi, S.; Belgacem, M. N.; Duarte, A. P.; Ben Salah, A.; Gandini, A. *Int. J. Adhes Adhes.* **2004**, *24* (1), 43−54.
(32) Abdelmouleh, M.; Boufi, S.; Belgacem, M. N.; Dufresne, A.; Gandini, A. *J. Appl. Polym. Sci.* **2005**, *98* (3), 974−984.
(33) Han, Y.; Li, W.; Zhang, J.; Meng, H.; Xu, Y.; Zhang, X. *RSC Adv.* **2015**, *5* (127), 104915−104922.
(34) Ventzki, R.; Rüggeberg, S.; Leicht, S.; Franz, T.; Stegemann, J. *Biotechniques.* **2007**, *42* (3), 271−279.
(35) Vlassakis, J.; Herr, A. E. *Anal. Chem.* **2017**, *89*, 12787−12796.
(36) Bansal, N. P.; Doremus, R. H. *Handbook of Glass Properties*; Elsevier Inc., 1986.
(37) Baselga, J.; Hernández-Fuentes, I.; Masegosa, R. M.; Llorente, M. A. *Polym. J.* **1989**, *21* (6), 467−474.
(38) Geldert, A.; Huang, H.; Herr, A. E. *Sci. Rep.* **2020**, *10* (1), 1−12.


https://doi.org/10.1021/acs.analchem.1c03919
*Anal. Chem.* 2022, 94, 2706−2712

# Supporting Information

## Electrotransfer of immunoprobes through thin-layer polyacrylamide gels

Andoni P. Mourdoukoutas† and Amy E. Herr*,‡

†The UC Berkeley/UCSF Graduate Program in Bioengineering, University of California, Berkeley, California, 94720, United States. ‡Department of Bioengineering, University of California, Berkeley, California, 94720, United States.
*Corresponding Author E-mail: aeh@berkeley.edu.

**SI EXPERIMENTAL SECTION**

**Chemicals, Reagents and Materials.** Acetic acid (#A6283, Honeywell), Methanol (#34860, Millipore Sigma), 3-(trimethoxysilyl)propyl methacrylate (#662275, Sigma-Aldrich), 30% T, 29:1C acrylamide/bis-acrylamide (#A3574, Sigma-Aldrich), N,N,N′,N′-tetramethylethylenediamine (TEMED, #T9281, Sigma-Aldrich), ammonium persulfate (APS, #A3678, Sigma-Aldrich), Rhodamine B (#R6626, Millipore Sigma), Ultrapure low melting point agarose (#16520050, Invitrogen), Donkey anti-Rabbit Alexa-Fluor 647 (#A31573, Invitrogen), Rhinohide™ (#R33400, Invitrogen). 10× Tris-glycine (#1610734, Bio-Rad), dichlorodimethylsilane (#440272, SigmaAldrich), microscope glass slides (#48300-026, VWR), N-[3-[(3-Benzoylphenyl)-formamido]propyl] methacrylamide in DMSO ("BPMA"; #PAL0603, PharmAgra Labs), SU-8 3050 (Microchem, now Kayaku Advanced Materials, Inc.), silicon wafers (#C04009, WaferPro), No. 0 glass cover slips (#CG00C, Thorlabs), # 1.5 glass cover slips (#0410A23, Thermo Scientific), Western Blot Roller (#84747, Thermo Fisher), Western blotting filter papers (#84783, Thermo Fisher Scientific), nanoporous membranes (regenerated cellulose, Spectra Por RC Dialysis Tubing, 3.5 kDa MWCO, #132725T, Fisher Scientific).

**Nanoporous Membrane and Glass Slide Silanization.** To facilitate covalent binding of polyacrylamide gel (10%T, 3.5C) to the nanoporous membranes, a nanoporous membrane silanization method was developed with inspiration from glass slide silanization protocols[1] and fabrication techniques for hybrid gel-cellulose materials.[2,3,4] First, the nanoporous membranes were cut into 25 x 37.5 mm single sheets (not tubes), soaked in ethanol for 48 hours, and air dried for 24 hours. Then, silane solution was prepared (previously described[1]) by mixing: 140 mL 3-(3-(trimethoxysilyl)propyl methacrylate), 210 mL acetic acid, 350 mL DI water. The silane solution was degassed in a sonicator for 10 min. Next, the nanoporous membranes were submerged in silane solution for 2 hrs, subsequently air dried for 48 hrs, then heated at 120C for 2 hrs in oxygen deprived atmosphere (vacuum furnace). Finally, nanoporous membranes were washed by agitating in baths of (1 min each bath): (1) methanol, (2) DI water, (3) methanol, (4) DI water. Silanized nanoporous membranes were stored with desiccant in a sealed container at 4ºC for up to a month until use. Glass slides were silanized as previously described[1]: (i) the same silane solution described above was prepared, (ii) glass slides were incubated in methanol for 30 min, (iii) glass slides were incubated in silane solution for 30 min, (iv) glass slides were washed by agitating in baths of (1 min each bath): (1) methanol, (2) DI water, (3) methanol, (4) DI water. Silanized glass slides were stored with desiccant in a sealed container at 20ºC for up to a month until use.

**SU-8 Coated Silicon Wafer Fabrication.** SU-8 features were patterned on a silicon wafer by photolithography as previously described.[1] Briefly, SU-8 features were cylindrical microposts 40 μm in height, 32 μm in diameter. To mitigate thin gel adhesion to the SU-8 mold, the SU-8 layer was coated with dichlorodimethylsilane as previously described.[1]

**TGNM Fabrication Process.** To fabricate the TGNM chip, first, the polyacrylamide gel precursor solution was prepared by mixing the following reagents: 30% T 29:1C acrylamide/bis-acrylamide (final concentration: 10% T), 10× Tris-glycine (10% v/v), BPMA (3% v/v), Rhinohide™ (final concentration: 4.66% v/v). The mixture was subsequently degassed and sonicated for 5 min and set aside until use. Next, the nanoporous membrane was adhered to a glass microscope slide by drying a hydrated nanoporous membrane onto a glass slide: (i) a silanized nanoporous membrane was hydrated by submerging in 1× Tris-glycine for 1 min, (ii) the hydrated nanoporous membrane was removed from the 1× Tris-glycine bath and layered onto a microscope glass slide, (iii) fluid and air pockets were removed from the hydrated nanoporous membrane by rolling the nanoporous membrane with a Western Blot Roller and allowing the nanoporous membrane to air dry. Then, to polymerize the thin polyacrylamide gel and graft the thin-gel to the nanoporous membrane: (i) chemical initiators of polymerization were added to the degassed and sonicated polyacrylamide gel precursor solution (final concentrations: 0.08% w/v APS, 0.08% w/v TEMED), (ii) the polyacrylamide gel precursor solution was then pipetted onto an SU-8 coated silicon wafer, (iii) a nanoporous membrane dried onto a glass slide was placed on top of SU-8 coated silicon wafer to mold the polyacrylamide gel precursor solution between the nanoporous membrane and the SU-8 coated silicon wafer, (iv) the polyacrylamide gel precursor solution was allowed to polymerize (20 min) and the TGNM glass assembly was removed from the SU-8 coated silicon wafer by sliding a razor between the glass slide and the SU-8 coated silicon wafer, (iv) the TGNM chip was released from the glass slide by sliding a razor between the glass slide and the nanoporous membrane and peeling the TGNM chip away from the glass slide. The TGNM chip was stored in 1× Tris-glycine at 4ºC for up to a week.

**Investigating the Fidelity of the TGNM Chip Fabrication Process.** TGNM chips were fabricated as described in the above section *TGNM fabrication process*, but with the inclusion of a fluorescent dye (0.001% w/v Rhodamine B) in the polyacrylamide gel precursor solution to visualize polymerized gel features. Thin gel glass chips were also fabricated following the same steps, but with no nanoporous membrane included. After thin gel polymerization, the thin gels were exposed to UV light for 45 s to photocapture Rhodamine B to the BPMA-functionalized thin gels (previously described[5]) and thin gels were subsequently diffusively washed in DI water for 1 hr to remove unbound Rhodamine B molecules. Imaging of the TGNM and thin-gel glass chips was performed by confocal microscopy through a #1.5 coverslip using a

Zeiss LSM 880 laser-scanning confocal microscope fitted with a 20× water dipping objective (NA=1.0, Zeiss W Plan APO 20x/1 DICIII). Final images were brightness and contrast-adjusted in Fiji75 (based on ImageJ76, National Institutes of Health) and Rhodamine B was used as a proxy for thin gel and nanoporous membrane location. Thin gel dimensions and features were manually identified and measured in Fiji75 using the *Measure* function. Analysis was performed in MATLAB®.

**Assessment of Nanoporous Membrane Electrical Conductivity Post-Silanization.** To evaluate the electrical conductivity of the separation material (either silanized nanoporous membrane, #0 glass cover slip, or no nanoporous membrane), an 'out-of-plane' electrotransfer system was assembled with the separation material sandwiched between two identical buffer reservoirs. First, the electrotransfer system was assembled: (i) 1 mm thick filter papers were cut to 15 x 15 mm squares and submerged in 1× Tris-glycine for 1 min, (ii) silanized nanoporous membranes were cut to 20 x 20 mm squares and submerged in 1× Tris-glycine for >5 min, (iii) two buffer-soaked filter papers (2 mm thickness total) were placed on a graphite electrode plate, (iv) depending on the material under investigation, one of the following separation materials the separation material under investigation (nanoporous membrane, glass, or no nanoporous membrane) was placed on top of the buffer reservoir and caution was observed to not trap air bubbles between the separation material and the buffer reservoir, (v) a second set of two buffer-soaked filter papers (2 mm thickness total) were placed on top of the separation material under investigation, (vi) a second graphite electrode plate was placed on top of the buffer reservoir sandwich and the electrode plates were separated by 4 mm shims placed on either side of the buffer reservoir sandwich. After the electrotransfer system was assembled, the system was connected to a power supply and an electric field was applied and electrical current was monitored: (i) the electrode plates were connected to a power supply (PowerPac Basic Power Supply, #1645050, BioRad), (ii) a constant voltage source of 20 V was applied from the power supply for a time duration of 60 s, (iii) the electrical current was recorded from the power supply over the duration of the applied voltage.

**Electrotransfer Probe Loading to TGNM Chips.** To implement electrotransfer probe loading in the TGNM chips, we first fabricated TGNM chips as described in the above section *TGNM fabrication process*. Next, we fabricated an antibody probe reservoir from 1.5% w/v low melting point agarose gel, as previously described[6]: (i) the following reagents were mixed and left on a 40ºC hotplate (to prevent agarose gelation) until use: 150 µL of molten 1.5% w/v low melting point agarose dissolved in 1× Tris-glycine, 5 µg of Donkey anti-Rabbit Alexa-Fluor 647, (ii) the molten agarose-probe mixture was cast into a 100 µm thick, 25 x 37.5 mm wide mold composed of an unsilanized nanoporous membrane, 100 µm shims, and a #1.5 glass cover slip, (iii) the mold was disassembled and the unsilanized nanoporous membrane was used to support the agarose-probe gel (the 'probe reservoir') until use. Then, we assembled an 'out-of-plane' electrotransfer system and probe was electrotransferred into the thin gel: (i) 1 mm thick filter papers were cut to 25 x 37.5 mm rectangles and submerged in 1× Tris-glycine for 1 min, (ii) two buffer-soaked filter papers (2 mm thickness total) were placed on a graphite electrode plate, (iii) the TGNM chip was placed on top of the buffer reservoir and caution was observed to not trap air bubbles between the TGNM chip and the buffer reservoir, (iv) the probe reservoir was layered onto the TGNM chip by using the unsilanized nanoporous membrane as a support to transport the probe reservoir, (v) a second set of two buffer-soaked filter papers (2 mm thickness total) were placed on top of the probe reservoir, (vi) a second graphite electrode plate was placed on top of the buffer reservoir sandwich and the electrode plates were separated by 4.1 mm shims placed on either side of the buffer reservoir sandwich, (vii) the electrode plates were connected to a power supply (PowerPac Basic Power Supply, #1645050, BioRad), (viii) a constant voltage source of 20 V was applied from the power supply for a time duration of 60 s. After probe delivery to the thin gel, the probe was immobilized in the thin gel and imaged: (i) the electrotransfer stack was disassembled and the TGNM chip was isolated and retrieved (caution was observed to retrieve only the TGNM chip, and to ensure that no probe reservoir remained on the thin gel surface), (ii) the TGNM chip was briefly (~2 s) dipped in 1× Tris-glycine to wash off excess probe remaining on the surface of the thin gel, (iii) the TGNM chips were exposed to UV light for 45 s to photocapture probe in-gel to the BPMA-functionalized thin gels (previously described[1,5]), (iv) the TGNM chips were imaged to assess probe fluorescence in-gel using a fluorescence microarray scanner (Genepix 4300A, Molecular Devices) and compared to TGNM chip fluorescence prior to probe delivery. Analysis of in-gel probe fluorescence images was performed using custom scripts in ImageJ and MATLAB®. To implement electrotransfer probe unloading in the TGNM chips, probe was first electrotransferred into the TGNM as described in steps (i) through (viii) of this section. After probe delivery to the thin gel, probe was electrotransfer unloaded from the TGNM by: (i) the electrotransfer stack was disassembled and the TGNM chip was isolated and retrieved (caution was observed to retrieve only the TGNM chip, and to ensure that no probe reservoir remained on the thin gel surface), (ii) the TGNM chip was submerged in 1× Tris-glycine to wash off excess probe remaining on the surface of the thin gel and rehydrate the TGNM with fresh buffer, (iii) the TGNM was removed from the 1× Tris-glycine bath and the 'out-of-plane' electrotransfer system was reassembled with fresh buffer soaked filter papers as described above, (iv) the electrode plates were connected to a power supply (PowerPac Basic Power Supply, #1645050, BioRad) such that the cathode (-) is more proximal to the nanoporous membrane layer than the thin gel layer of the TGNM, (viii) a constant voltage source of 20 V was applied from the power supply for a time duration of 60 s. After probe delivery to the thin gel, the probe was immobilized in the thin gel and imaged as described above.

**Diffusive Probe Loading to TGNM Chips.** To implement diffusive probe loading in the TGNM chips, we fabricated TGNM chips as described in the above section *TGNM fabrication process*, with the exception that the TGNM chips were not removed from the glass slide support used during chip fabrication. The TGNM assembly facilitates replication of the conventional diffusive probing strategies used in thin-gel glass chips. First, a probe solution was made by mixing the following reagents (per 25 x 37.5 mm chip): 50 µL of 1× Tris-glycine, 5 µg of Donkey anti-Rabbit Alexa-Fluor 647. Then, the probe solution was pipette onto a glass plate. Next, the TGNM glass chip was placed onto the probe solution (thin gel interfaced with probe). The system was covered by a humid, dark chamber at 20ºC and unperturbed for the diffusive incubation time under investigation (either 1 min or 1 hr). After completion of the diffusive incubation time, the TGNM glass chip was retrieved and briefly (~2 s) dipped in 1× Tris-glycine to wash off excess probe remaining on the surface of the thin gel. The TGNM chips were exposed to UV light for 45 s to photocapture probe in-gel to the BPMA-functionalized thin gels (previously described[1,5]) and the TGNM glass chips were imaged to assess probe fluorescence in-gel using a fluorescence microarray scanner (Genepix 4300A, Molecular Devices) and compared to TGNM glass chip fluorescence prior to probe delivery. Analysis of in-gel probe fluorescence images was performed using custom scripts in ImageJ and MATLAB®.

**NOTE S1: Diffusion Coefficient for Antibody Probe in 10%T Polyacrylamide Gel**
Diffusion coefficient of antibody probe in free solution ($D_{H_20}$) is calculated using Stokes-Einstein equation

$$D_{H_20} = \frac{k_B T}{6\pi\eta_{H_20} R_h}$$

where $k_B$ is Boltzman's constant, T is temperature, $\eta_{H_20}$ is viscosity of water, $R_h$ is the hydrodynamic radius of the migrating antibody probe. The hindered diffusion of the antibody probe in polyacrylamide gel ($D_{gel}$) is given by[7]

$$D_{gel} = D_{H_20} \times \exp\left(-3.03 {R_h}^{0.59} \times \%T^{0.94}\right)$$

where $\%T$ is the polyacrylamide gel density. The diffusion coefficient of an antibody probe ($R_h$ = 50 Å) in a 10%T gel ( $\%T$ = 10) results in $D_{gel} \approx$ 1.40 µm$^2$/s .

**NOTE S2: Electrokinetic Theory and Electromigration of Antibody Isotype Classes.**
Antibody electromigration velocity (v; µm s$^{-1}$) is linearly proportional to the applied electric field strength (E; V cm$^{-1}$) and antibody electrophoretic mobility (µ; cm$^2$ V$^{-1}$s$^{-1}$)

$$v = \mu * E$$

Antibody µ is given by

$$\mu = \frac{q}{(6\pi\eta R_h)} 10^{-K_r \%T}$$

Where q (C) is the net charge of the antibody molecule, η (Pa s$^{-1}$) is the solution viscosity, $R_h$ (nm) is the hydrodynamic radius of the antibody molecule, Kr is the gel retardation coefficient, and %T (% acrylamide monomer) is the gel density.[8] For antibody electromigration under native buffer conditions, the antibody µ varies with changes in the antibody $R_h$ and q, which can exist across antibody isotype classes (e.g. IgG vs. IgM). However, minimal variation in µ is expected for antibody species of the same isotype, as there typically exists much less variation in $R_h$ and q of antibodies within an isotype class than across classes.[9] Similarly, while fluorophore conjugation of antibodies can alter the effective $R_h$ and q of the antibody, antibody conjugation is not expected to adversely impact antibody electromigration, as (i) compared to antibody size (150 kDa for IgG) fluorophore tags are quite small (<1 kDa, <1% molecular mass of the antibody) (Alexa Fluor 488 Protein Labelling Kit, https://www.thermofisher.com/order/catalog/product/A10235, accessed 26 October 2021) and (ii) antibodies and fluorophores both typically carry net negative q in native conditions, meaning conjugated antibody are expected to exhibit increased µ magnitude and v.[10]

**NOTE S3: Electrical Current Decay in Electrotransfer Systems**

The decay in electrical current measured is attributed to gas products of electrolysis that form at the electrode plates, which would increase the resistivity of the buffer reservoirs over time.[6,11] Additionally, the electrical current time de- cay may be caused by liquid evaporation from the buffer reservoir as a result of Joule heating (ohmic heating) in the electrotransfer configuration.[12,13,14] Time-varying buffer reservoir resistivity and Joule heating in the electrotransfer configuration can degrade probe electrotransfer performance, including non- uniform probe electromigration across the nanoporous membrane surface or probe molecule denaturation via excessive system heating, as has been described in previous electrotransfer systems.[11,15] Further study would build on the engineering design of similar electrotransfer systems to mitigate the adverse impacts of Joule heating and electrolysis on molecular transport.[6,16]

## REFERENES


1. Kang C-CC, Yamauchi KA, Vlassakis J, Sinkala E, Duncombe TA, Herr AE. Single cell-resolution western blotting. *Nat Protoc*. 2016;11(8):1508-1530. doi:10.1038/nprot.2016.089
2. Abdelmouleh M, Boufi S, ben Salah A, Naceur Belgacem M, Gandini A. Interaction of Silane Coupling Agents with Cellulose. *Langmuir*. 2002;18:3203-3208. doi:10.1021/la011657g
3. Abdelmouleh M, Boufi S, Belgacem MN, Duarte AP, Ben Salah A, Gandini A. Modification of cellulosic fibres with functionalised silanes: Development of surface properties. *Int J Adhes Adhes*. 2004;24(1):43-54. doi:10.1016/S0143-7496(03)00099-X
4. Abdelmouleh M, Boufi S, Belgacem MN, Dufresne A, Gandini A. Modification of cellulose fibers with functionalized silanes: Effect of the fiber treatment on the mechanical performances of cellulose-thermoset composites. *J Appl Polym Sci*. 2005;98(3):974-984. doi:10.1002/app.22133
5. Dormán G, Nakamura H, Pulsipher A, Prestwich GD. The Life of Pi Star: Exploring the Exciting and Forbidden Worlds of the Benzophenone Photophore. *Chem Rev*. 2016;116(24):15284-15398. doi:10.1021/acs.chemrev.6b00342
6. Mourdoukoutas AP, Grist SM, Herr AE. Rapid electrotransfer probing for improved detection sensitivity in in-gel immunoassays. *Anal Methods*. 2020;12(38). doi:10.1039/d0ay01203c
7. Park H, Johnson CS, Gabriel ' DA. Probe Diffusion in Polyacrylamide Gels As Observed by Means of Holographic Relaxation Methods: Search for a Universal Equation. *Macromolecules*. 1990;23:1548-1553. https://pubs.acs.org/doi/pdf/10.1021/ma00207a052. Accessed March 17, 2018.
8. Ferguson K. Starch-gel Electrophoresis - Application to the Classification of Pituitary Proteins and Polypeptides. *Metab, Clin Exp*. 1964;13:985-1002. http://www.his.com/~djt/FergusonKA-Metabolism-October-1964.pdf. Accessed April 5, 2018.
9. Vidarsson G, Dekkers G, Rispens T. IgG subclasses and allotypes: From structure to effector functions. *Front Immunol*. 2014;5(OCT). doi:10.3389/fimmu.2014.00520
10. Zanetti-Domingues LC, Tynan CJ, Rolfe DJ, Clarke DT, Martin-Fernandez M. Hydrophobic Fluorescent Probes Introduce Artifacts into Single Molecule Tracking Experiments Due to Non-Specific Binding. *PLoS One*. 2013;8(9). doi:10.1371/journal.pone.0074200
11. Ventzki R, Rüggeberg S, Leicht S, Franz T, Stegemann J. Comparative 2-DE protein analysis in a 3-D geometry gel. *Biotechniques*. 2007;42(3):271-279. doi:10.2144/000112421/ASSET/IMAGES/MEDIUM/FIGURE1.JPG
12. Grist SM, Mourdoukoutas AP, Herr AE. 3D projection electrophoresis for single-cell immunoblotting. *Nat Commun 2020 111*. 2020;11(1):1-17. doi:10.1038/s41467-020-19738-1
13. Vlassakis J, Herr AE. Joule Heating-Induced Dispersion in Open Microfluidic Electrophoretic Cytometry. *Anal Chem*. 2017;89:12787-12796. doi:10.1021/acs.analchem.7b03096
14. Zhu L, Tangrea MA, Mukherjee S, Emmert-Buck MR. Layered Electrophoretic Transfer – A Method for Pre-Analytic Processing of Histological Sections. *Proteomics*. 2011;11(5):883-889. doi:10.1002/pmic.201000476
15. Bansal NP, Doremus RH. *Handbook of Glass Properties*. Elsevier Inc.; 2013.
16. Grist SM, Mourdoukoutas AP, Herr AE. 3D projection electrophoresis for single-cell immunoblotting. *bioRxiv*. October 2019:doi: https://doi.org/10.1101/805770. doi:10.1101/805770